Society for Mathematical Biology

Turing Instabilities and Rotating Spiral Waves in Glycolytic Processes

Luis A. Cisneros-Ake[1] · **Juan C. Gonzalez-Rodriguez[2]** ·
Laura R. González-Ramírez[1]

Abstract

We study single-frequency oscillations and pattern formation in the glycolytic process modeled by a reduction in the well-known Sel'kov's equations (Sel'kov in Eur J Biochem 4:79, 1968), which describe, in the whole cell, the phosphofructokinase enzyme reaction. By using averaging theory, we establish the existence conditions for limit cycles and their limiting average radius in the kinetic reaction equations. We analytically establish conditions on the model parameters for the appearance of unstable nonlinear modes seeding the formation of two-dimensional patterns in the form of classical spots and stripes. We also establish the existence of a Hopf bifurcation, which characterizes the reaction dynamics, producing glycolytic rotating spiral waves. We numerically establish parameter regions for the existence of these spiral waves and address their linear stability. We show that as the model tends toward a suppression of the relative source rate, the spiral wave solution loses stability. All our findings are validated by full numerical simulations of the model equations. Finally, we discuss in vitro evidence of spatiotemporal activity patterns found in glycolytic experiments, and propose plausible biological implications of our model results.

Keywords Glycolysis · Oscillations · Turing instabilities · Spiral waves

✉ Luis A. Cisneros-Ake
lacisnerosa@ipn.mx

Juan C. Gonzalez-Rodriguez
juancarlosgonzalez1994@gmail.com

Laura R. González-Ramírez
lrgonzalezr@ipn.mx

[1] Departamento de Matemáticas, ESFM, Instituto Politécnico Nacional, Unidad Profesional Adolfo López Mateos Edificio 9, 07738 Mexico, Mexico

[2] Posgrado en Ciencias Fisicomatemáticas, ESFM, Instituto Politécnico Nacional, Unidad Profesional Adolfo López Mateos Edificio 9, 07738 Mexico, Mexico

⚛ Springer

1 Introduction

Sustained periodic oscillations have been observed in different biochemical systems of varying complexity (Hess and Boiteux 1971; Olsen and Degn 1978; Gray and Scott 1990). In particular, glycolytic oscillations in yeast cell extracts and yeast cell populations have been widely reported (Goldbeter and Lefever 1972; Murray et al. 2007; Weber et al. 2020). Understanding the exact conditions permitting the appearance and regulation of such oscillations is an important problem that has been pursued in both experimental settings and mathematical models (Weber et al. 2020; Bier et al. 2000). Glycolysis is the fundamental biochemical process in the metabolic pathway that explains how living cells may obtain energy by breaking down glucose. More specifically, the glycolytic process, taking place in the cytosol, describes how glucose is transformed into pyruvate (pyruvic acid) in a sequence of typically ten enzyme-catalyzed reactions. As a result of the free energy released during the whole process, adenosine triphosphate (ATP) is additionally produced along with pyruvate. The most prominent catalyzing enzymes hexokinase and phosphofructokinase play their role in the glycolytic intermediate reactions for the conversions of glucose into glucose-6-phosphate and fructose-6-phosphate into fructose 1,6-bisphosphate, respectively (Goldbeter 1996; Voet et al. 2006). Additionally, different coenzymes participate during glycolytic sugar degradation; among them, nicotinamide adenine dinucleotide (NAD) plays a central role. This coenzyme can be present in both oxidized (NAD^+) and reduced form (NADH). The availability of NAD^+ is decisive in the regular development of the glycolysis, whereas NADH is produced during the glycolytic energy-release stage. Throughout the glycolytic pathway, NADH molecules enter a feedback cycle and fluctuate between the oxidized and reduced states. In particular, if NAD^+ is not obtainable, the glycolytic process can slow down or totally stop. Therefore, the dynamics of NAD are essential to infer information about the glycolytic dynamics (Casem 2016).

In the middle of the last century, one of the first biochemical oscillations were found in the glycolysis process that takes place in metabolic systems. In this context, E. E. Sel'kov, in his seminal paper (Sel'kov 1968), studied the problem of single-frequency sustained oscillations by means of a kinetic model of a simplified enzyme reaction. In his five-variable model, an enzyme (e) is inhibited by a monosubstrate (s_1) and activated by a monoproduct (s_2). The remaining variables determine the information regarding the enzyme substrate complex and the inactivated enzyme. By considering a limiting process, Sel'kov obtained a reduction from his five-variable model to a two-variable model to describe the main features relative to the concentrations of the substrate and the product during the enzyme reaction. The biological motivation of the previous models relies on experimental observations of the phosphofructokinase enzyme reaction as a source of glycolytic oscillations. During this reaction, there exists inhibition to the enzyme due to a substrate, ATP, and activation of the enzyme mainly by a product, adenosine diphosphate (ADP). Indeed, Sel'kov's model was found to qualitatively describe most of the experimental conditions on single-frequency oscillations in the glycolytic process when the phosphofructokinase enzyme was considered, thus improving the previous studies of Higgins (1964, 1965). Dynamical equations describing the previous reaction, at very low flux rates, can be obtained from a sim-

plified version of Sel'kov's five-variable model (Ashkenazi and Othmer 1978). The kinetic equations used in Ashkenazi and Othmer (1978) to describe single-frequency oscillations in the glycolysis process are:

$$\frac{\mathrm{d}u}{\mathrm{d}t} = f(u, v) = -u + v\left(a + u^2\right), \tag{1}$$

$$\frac{\mathrm{d}v}{\mathrm{d}t} = g(u, v) = b - v\left(a + u^2\right), \tag{2}$$

where $a \geq 0$ is the dimensionless rate constant for the low activity state and $b > 0$ is the dimensionless input flux (relative source rate), while u and v are the average concentrations of the substrate inhibition (ATP) and product activation (ADP), respectively. In this model, it is assumed that the enzyme reaction exhibits two states: a low activity state and a high activity product-activated state. We also note that in this formulation as $a \to 0$, we tend toward a version of the two-variable Sel'kov's model (Sel'kov 1968). Another approach, focusing on the allosteric regulation of the phosphofructokinase instead of the whole glycolytic pathway, was developed by Goldbeter and Lefever (1972) for the ATP (inhibitor) and the ADP (allosteric activator) of the phosphofructokinase. However, Goldbeter's model presents more complex reaction interactions than Sel'kov's two-variable model, making it difficult for mathematical treatment.

Organized patterns of activity—in the form of spots, stripes and spirals—have been observed in both chemical and biological systems (Maini et al. 1997). These patterns can be generated by the latency of nonlinear interactions, such as it occurs during the glycolytic pathway, and transport processes (Nicolis and Prigogine 1977; Zaikin and Zhabotinsky 1970). In Mair and Müller (1996), Mair et al. (2001), Vermeer (2008), Müller et al. (1985, 1987), we find reports of in vitro experimental evidence of the emergence of spatiotemporal patterns of NADH activity during glycolytic reactions. Such patterns vary in complexity, from propagating glycolytic traveling waves and propagating glycolytic spiral waves to more complex stationary patterns. In particular, Turing-like patterns in the form of mosaic-like patterns were observed in Müller et al. (1985, 1987). These transient patterns can qualitatively resemble Turing's "stripes." Also, the work developed in Vermeer (2008) reported the evolution of dot-shaped waves and short-distance propagating waves. Such patterns can also qualitatively resemble Turing's "spots." Due to the previously mentioned relevance of the NADH production during glycolysis, it is believed that NADH patterns are essential key factors that determine glycolytic spatiotemporal oscillations (Mair and Müller 1996; Mair et al. 2001; Vermeer 2008; Corkey et al. 1988). Moreover, it has been suggested that through these patterns, glycolysis plays a role in the processing of biological information. For instance, experimental observations have determined a relation between spatiotemporal glycolytic oscillations and insulin secretion of β cells in pancreatic islets (Corkey et al. 1988). Additionally, it has been established a connection between the propagation of NADH waves and the propagation direction of immune system's activated neutrophil cells (Petty et al. 2000). Also, an experimental setting developed in Bulusu et al. (2017) has established that spatiotemporal glycolytic dynamics are linked to the development of organogenesis in mouse embryos. Due to all of the pre-

viously mentioned experimental evidence and, in order to understand the plausible role of glycolysis in the processing of biological information, it is of importance to determine theoretical conditions that allow the propagation of spatiotemporal activity patterns and stationary activity patterns.

The main goal of this manuscript is to establish conditions for the existence of single-frequency oscillations and two-dimensional spatial pattern formation in the glycolytic process. To do so, Sect. 2 addresses on the existence of single-frequency oscillations in the dynamics of the kinetic reactions describing the model. Here, we propose a novel approach by considering the averaging theory on periodic solutions. By using this approach, we successfully recover the limiting average radius of the limit cycle, as well as its stability. In Sect. 3, by considering a spatially extended version of the glycolytic model, we establish conditions for Turing pattern formation, and we exhibit examples showing the appearance of spots and stripes of activity. In Sect. 4, we show an existence region of spiral waves of activity in the glycolytic model by considering a two-parameter numerical continuation of a stationary problem. We also address the linear stability of such solutions and relate the existence of spiral solutions determined by stationary solutions in a rotating frame to spiral solutions in the full system of equations. Finally, in Sect. 5, we discuss plausible biological implications of our work, according to the experimental evidence, and we present our concluding remarks.

2 Dynamics of Kinetic Reactions

We start our analysis of the model Eqs. (1)–(2) by reproducing the well-known result on the existence of a Hopf bifurcation. We first notice that the system (1)–(2) only holds an equilibrium state at $(u^*, v^*) = (b, \frac{b}{a+b^2})$, whose stability explains the oscillatory behavior in the glycolytic process. This type of periodic evolution is required for the possibility of having a Hopf bifurcation, which accounts for the transition to an isolated periodic orbit. In contrast to the traditional stability analysis, we use the averaging theory for periodic systems (Sanders and Verhulst 1985; Chow and Mallet-Paret 1977) to reproduce the model parameter conditions where the Hopf bifurcation takes place. This theory affirms that a perturbed periodic system may be replaced, to order one in the perturbation parameter, by its corresponding angular averaging in the appropriate time scales (Chow and Mallet-Paret 1977). In the context of our biological model, the dimensionless rate constant, a, plays the role of the perturbation parameter. Following this theory, we use polar coordinates around the only equilibrium point (u^*, v^*). That is, we consider the change of variables $u = u^* + r \cos \theta$ and $v = v^* + r \sin \theta$ into Eqs. (1)–(2) to find the corresponding action-angle simplified system,

$$\frac{\mathrm{d}r}{\mathrm{d}t} = \left(-1 + 2u^*v^*\right) r \cos^2 \theta + \left(a + u^{*2}\right) r \sin \theta \cos \theta + v^* r^2 \cos^3 \theta + r^3 \sin \theta$$
$$\cos^3 \theta + 2u^* r^2 \sin \theta \cos^2 \theta - 2u^* v^* r \sin \theta \cos \theta - \left(a + u^{*2}\right) r \sin^2 \theta$$
$$- v^* r^2 \cos^2 \theta \sin \theta - 2u^* r^2 \cos \theta \sin^2 \theta - r^3 \sin^2 \theta \cos^2 \theta \equiv F\left(r, \theta\right), \quad (3)$$

$$\frac{d\theta}{dt} = \left(1 - 2u^*v^*\right) \sin\theta \cos\theta - \left(a + u^{*2}\right) \sin^2\theta$$

$$- v^*r \sin\theta \cos^2\theta - 2u^*r \sin^2\theta \cos\theta$$

$$- r^2 \sin^2\theta \cos^2\theta - 2u^*v^* \cos^2\theta - \left(a + u^{*2}\right) \cos\theta \sin\theta - 2u^*r \cos^2\theta \sin\theta$$

$$- v^*r \cos^3\theta - r^2 \sin\theta \cos^3\theta \equiv G\left(r, \theta\right). \tag{4}$$

In the averaging theory, one then considers the average system in θ around a cycle on $[0, 2\pi]$. We thus consider the average variation $\bar{r}$ in the form

$$\frac{d\bar{r}}{dt} = \frac{1}{2\pi} \int_0^{2\pi} F(\bar{r}, \theta) d\theta = \frac{\bar{r}}{2} \left(-1 + 2u^*v^* - a - u^{*2} - \frac{\bar{r}^2}{4}\right)$$

$$= \frac{\bar{r}}{2} \left(\frac{-a + b^2 - \left(a + b^2\right)^2}{a + b^2} - \frac{\bar{r}^2}{4}\right). \tag{5}$$

Then, the local periodic behavior of the original system (1)–(2) around the equilibrium point (u^*, v^*) is approximately predicted for a small average radius $\bar{r}$. Thus, the previous equation near the equilibrium at $\bar{r} = 0$ becomes:

$$\frac{d\bar{r}}{dt} = \left(\frac{-a + b^2 - \left(a + b^2\right)^2}{a + b^2}\right) \frac{\bar{r}}{2} \equiv \Delta \frac{\bar{r}}{2}. \tag{6}$$

The solution of Eq. (6) is $\bar{r}(t) = A \exp\left(\frac{\Delta}{2}t\right)$, where $A = constant$. The previous solution indicates the occurrence of a Hopf bifurcation at $\Delta = 0$, where the equilibrium (u^*, v^*) changes its stability from an unstable spiral when $\Delta > 0$ to a stable spiral for $\Delta < 0$. That is, the two-parameter relationship:

$$\Delta = 0, \text{ or, } b^2 = \frac{-2a + 1 \pm \sqrt{1 - 8a}}{2}, \tag{7}$$

defines a parabolic parameter region for the model where a stable limit cycle takes place, see Fig. 1a. The same result is obtained, for example, in Strogatz (1994) using the traditional local (linear) stability analysis and Poincaré's theorem. The existence of the limit cycle agrees with the fact that the glycolysis process proceeds in an oscillatory fashion due to the formation and breakdown of glucose. An approximation to the average radius of the limit cycle is actually obtained from Eq. (5) as the nonzero equilibrium solution at $\bar{r} = 2\sqrt{\Delta}$, see Fig. 1b. Also, the relationship between the kinetic parameters recovers the well-known conditions for the existence on the limit cycles on the two-variables Sel'kov model ($a = 0$), where the source rate, b, needs to be close to one. It is worth mentioning that, in contrast to the linear analysis, our averaging approximation not only predicts the Hopf bifurcation but also provides an order one approximation for the size of the limit cycle and its stability. Therefore, under this approach as the source rate is varied, we obtain an estimation of quantitative features of the glycolytic oscillations.

(a)

(b)
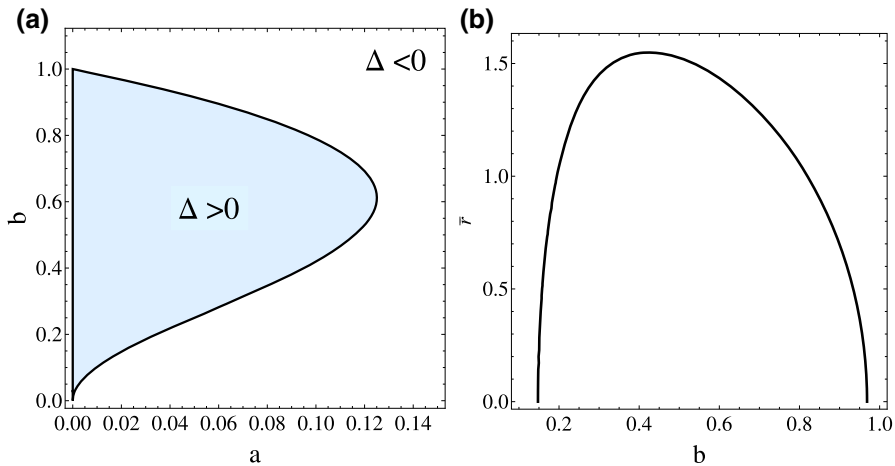
Fig. 1 Hopf bifurcation: **a** parabolic parameter region obtained from Eq. (7). The region $\Delta > 0$ determines unstable spiral equilibrium points and $\Delta < 0$ determines stable equilibrium points, respectively. **b** Approximation to the radius of the limit cycle $\bar{r}(b) = 2\sqrt{\Delta}$ for $a = 0.02$

For illustrative purposes, we now numerically solve Eqs. (1)–(2) using a fourth-order Runge–Kutta method for convenient initial conditions. Figure 2a shows the phase plane (u, v) indicating the existence of a limit cycle, as predicted from the bifurcation analysis for the model parameters $a = 0.02$ and $b = 0.2$. The size of such limit cycle is well-approximated from $\bar{r}(b)$, as Fig. 1b indicates. On the other hand, Fig. 2b, c depicts the temporal evolution of the concentrations u and v obtained from the initial conditions $u(0) = 1.5$, $v(0) = 1$ and $u(0) = 0.5$, $v(0) = 4$ corresponding to inner and outer orbits around the associated limit cycle. The behavior shown in Fig. 2 characterizes the self-sustained oscillatory evolutions predicted in early publications on the glycolytic process.

The rest of the paper is devoted to analyze the two-dimensional spatial diffusion of the concentrations u and v obeying the kinetic reactions (1)–(2). As far as the authors are aware, a detailed analysis of this problem has not been undertaken in the literature yet. Our purpose is to show how the stable limit cycle appearing in the reaction equations influence the dynamics in the spatial diffusion of the two concentrations. We show that Turing instabilities give place to spots and stripes patterns, while spiral waves may arise in the model parameters where there is a limit cycle.

3 Reaction–Diffusion Interactions: Pattern Formation

Assuming that the transport of the ATP and the ADP in the spatial domain occurs by passive diffusion, determined by fixed constants $D_u > 0$ and $D_v > 0$, we obtain the following reaction–diffusion model:

$$\frac{\partial u}{\partial t} = D_u \nabla^2 u + f(u, v) = D_u \nabla^2 u - u + v\left(a + u^2\right), \tag{8}$$

(a)

(b)

(c)
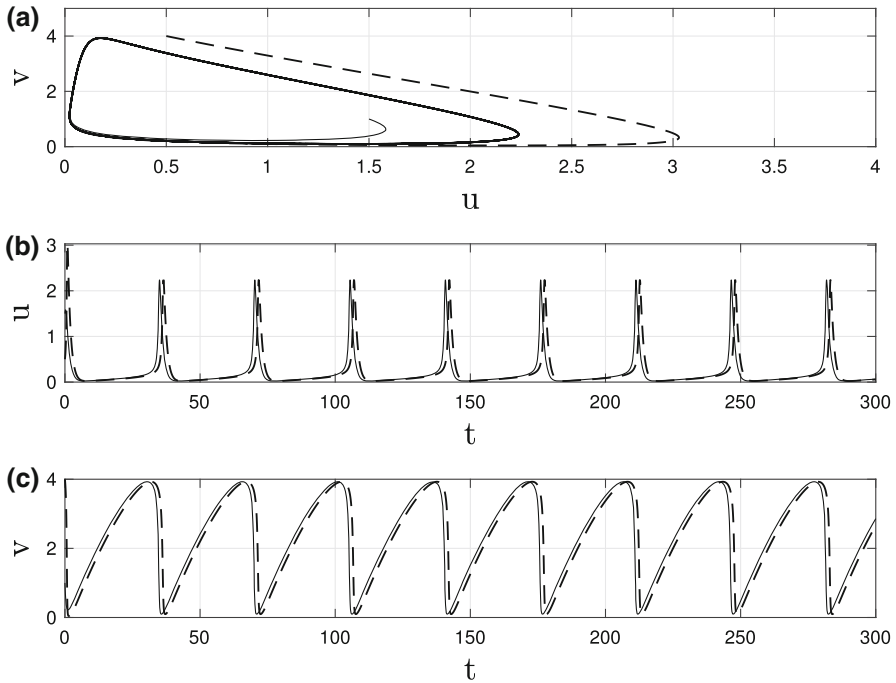
Fig. 2 Numerical solution of Eqs. (1)–(2) for $a = 0.02$ and $b = 0.2$. **a** Phase plane (u, v). **b** Solution $(t, u(t))$ and **c** solution $(t, v(t))$. Continuous curves for the initial condition $u(0) = 1.5$, $v(0) = 1$ and dash curves for $u(0) = 0.5$, $v(0) = 4$

$$\frac{\partial v}{\partial t} = D_v \nabla^2 u + g(u, v) = D_v \nabla^2 v + b - v\left(a + u^2\right), \tag{9}$$

where ∇^2 is the Laplace operator in D spatial dimensions. Equations (8)–(9) are considered in the unit rectangle $[0, 1]^D$ since the scaling over an arbitrary rectangle $[0, L]^D$ just adds an extra factor of D/L^2 in front of the Laplacian. Thus, in D-dimensions, it is possible to redefine the diffusion coefficients as $D_u \rightarrow D_u \frac{D}{L^2}$ and $D_v \rightarrow D_v \frac{D}{L^2}$ to absorb the spatial scalings. In this work, we focus on the two-dimensional case $D = 2$. Also, to address the classical pattern formation problem, we consider no-flux boundary conditions $u_x(0, y) = v_x(0, y) = 0$, $u_x(1, y) = v_x(1, y) = 0$; and $u_y(x, 0) = v_y(x, 0) = 0$, $u_y(x, 1) = v_y(x, 1) = 0$. We are specially interested in establishing model parameter conditions, including diffusivities coefficients, allowing for the pattern formation in the different scenarios of Turing instabilities and spiral rotating waves, as it is explained below.

3.1 Turing Instabilities

We start following Turing's criteria in our model equations for diffusion to cause instabilities in the only stable equilibrium state. As we mentioned above, in the absence of diffusion, $D_u = D_v = 0$, the corresponding reaction system (1)–(2) has a stable equilibrium point at (u^*, v^*) when the following two conditions are satisfied

$$f_u(u^*, v^*) + g_v(u^*, v^*) < 0, \tag{10}$$

$$f_u(u^*, v^*)g_v(u^*, v^*) - f_v(u^*, v^*)g_u(u^*, v^*) > 0, \tag{11}$$

where subscripts denote partial derivatives. Since diffusion has a smoothing effect, Alan Turing asked whether diffusion can destabilize a system from a homogeneous stable steady state (Turing 1952). To answer this question, one needs to linearize the full PDE system (8)–(9) around the equilibrium point (u^*, v^*) in the form $u(x, y, t) = u^* + e^{\lambda t}\eta(x, y)$, $v(x, y, t) = v^* + e^{\lambda t}\mu(x, y)$ for $\eta, \mu \ll 1$, to find the eigenvalue problem:

$$\lambda \begin{bmatrix} \eta \\ \mu \end{bmatrix} = \underbrace{\begin{bmatrix} f_u - \kappa^2 D_u & f_v \\ g_u & g_v - \kappa^2 D_v \end{bmatrix}}_{M} \begin{bmatrix} \eta \\ \mu \end{bmatrix},$$

for the wave number κ satisfying $\kappa^2 = \kappa_x^2 + \kappa_y^2$ where $\kappa_x = n\pi$ and $\kappa_y = m\pi$ are the wave numbers in the x and y directions, respectively. Thus, the diffusive effects are taken into account as a perturbation of the original Jacobian in the reaction system through the introduction of the wave number κ. In this way, Turing instabilities take place when κ is such that the matrix M accepts eigenvalues with positive real part, that is, when $\text{tr}(M) > 0$ or $\det(M) < 0$. By considering the condition (10), we obtain that $\text{tr}(M) = f_u + g_v - \kappa^2 (D_u + D_v) < 0$. We thus only have to satisfy,

$$h\left(\kappa^2\right) = \det(M) = D_u D_v \kappa^4 - (D_v f_u + D_u g_v)\kappa^2 + f_u g_v - f_v g_u < 0. \tag{12}$$

Since $h\left(\kappa^2\right)$ is parabolic in κ^2 and opening upward, real wave numbers are obtained when there exist positive real solutions of $h\left(\kappa^2\right) = 0$. We thus obtain the following two conditions for Turing instabilities:

$$df_u + g_v > 0, \tag{13}$$

$$(df_u + g_v)^2 > 4d (f_u g_v - f_v g_u), \tag{14}$$

where $d = D_v/D_u > 0$ is the diffusion ratio. We may notice that $d \neq 1$ otherwise the conditions (10) and (13) contradict each other. Also, Eqs. (10) and (13) imply that f_u and g_v have opposite signs, that is, $f_u g_v < 0$. Thus, from Eq. (11), we must have $f_v g_u < 0$.

In the case of the glycolysis model, the conditions (10)–(11) are satisfied for $-a + b^2 < (a + b^2)^2$ or $\Delta < 0$, see Fig. 1. On the other hand, Turing's conditions given by Eqs. (13)–(14) applied to the glycolysis model yield,

$$d\left(b^2 - a\right) > \left(b^2 + a\right)^2, \tag{15}$$

$$\left[d\left(b^2 - a\right) - \left(b^2 + a\right)^2\right]^2 > 4d\left(b^2 + a\right)^3. \tag{16}$$
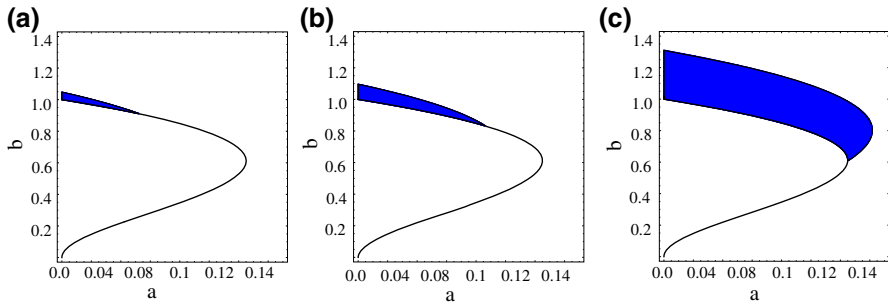
Fig. 3 Turing's instability region obtained from Eqs. (15)–(16) for **a** $d = 6.4$, **b** $d = 8$ and **c** $d = 10$

Our previous observations lead to $d > 0$ and $d \neq 1$, implying that in order to obtain Turing patterns in the glycolysis model the diffusivities of the product and substrate need to be sufficiently unequal. We now proceed to numerically analyze the Turing regions determined by $\Delta < 0$ in Eqs. (15) and (16). In Fig. 3, we show examples of the Turing instability region for different diffusion rates. We find that as the diffusivity of the product is near to 6.2 times stronger than the diffusivity of the substrate, Turing patterns emerge. Our results in Fig. 3 provide a scenario in which glycolytic Turing patterns emerge under sufficiently strong diffusivity of the product, sufficiently large source rate, and a sufficiently low rate constant for the low activity state.

In order to validate our findings, we numerically solve the full reaction diffusion system (8)–(9) by means of a second-order central difference scheme in space and a first-order forward difference approximation in time (Strikwerda 2004), with the steps $\delta x = \delta y = 0.01$ and $\delta t = 0.001$, which is adapted into the MEX-CUDA environment of MATLAB due to the amount of computational work. It is worth to mention that the discretization of the Laplacian is embedded in CUDA, while the temporal iterations are dealt in a MATLAB code. Additionally, in all of our numerical simulations, we are taking initial conditions as perturbations by uniformly distributed random numbers in $[0, \epsilon]$, for sufficiently small ϵ, of the only equilibrium (u^*, v^*). Thus, we are choosing, for example, parameter values in the shaded region of Fig. 3b (that is, the diffusivity of the product is acting 8 times faster than the diffusivity of the substrate) to get two-dimensional patterns of the Turing type. The first scenario corresponds to relatively small wave numbers κ. For instance, taking $a = 0.1$, $b = 0.85$ and $D_u = 0.0025$ into the condition (12) provides $48.8 \leq \kappa \leq 80.3$ or $10.6 \leq n^2 + m^2 \leq 15.8$. It is easily seen that this last condition is only satisfied for $(n, m) = (3, 2)$ or $(n, m) = (2, 3)$ where n and m indicate the number (integer) of oscillations in the x and y directions, respectively. Figure 4 displays the full numerical evolution of Eqs. (8)–(9) for a perturbed initial condition u and v obtained from these model parameters. From this simulation, we may observe how this temporal evolution leads to $(3, 2)$ spots in Fig. 4c, d, as it was previously predicted. On the other hand, the model parameters $a = 0.025$, $b = 0.961$ and $D_u = 0.0001$ yield, from Eq.(12), the condition $186.2 \leq n^2 + m^2 \leq 653.3$ which allows several large enough integer values for n and m. In this case, the larger number of allowed spots are packed in the form of stripes oriented in different directions. For instance, Fig. 5 shows a particular arrangement of
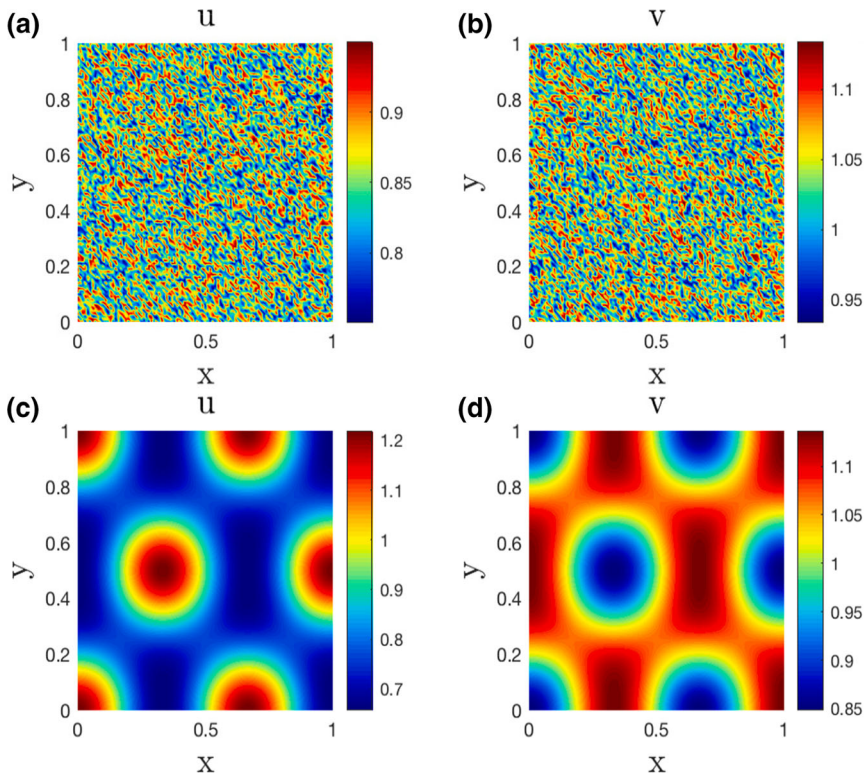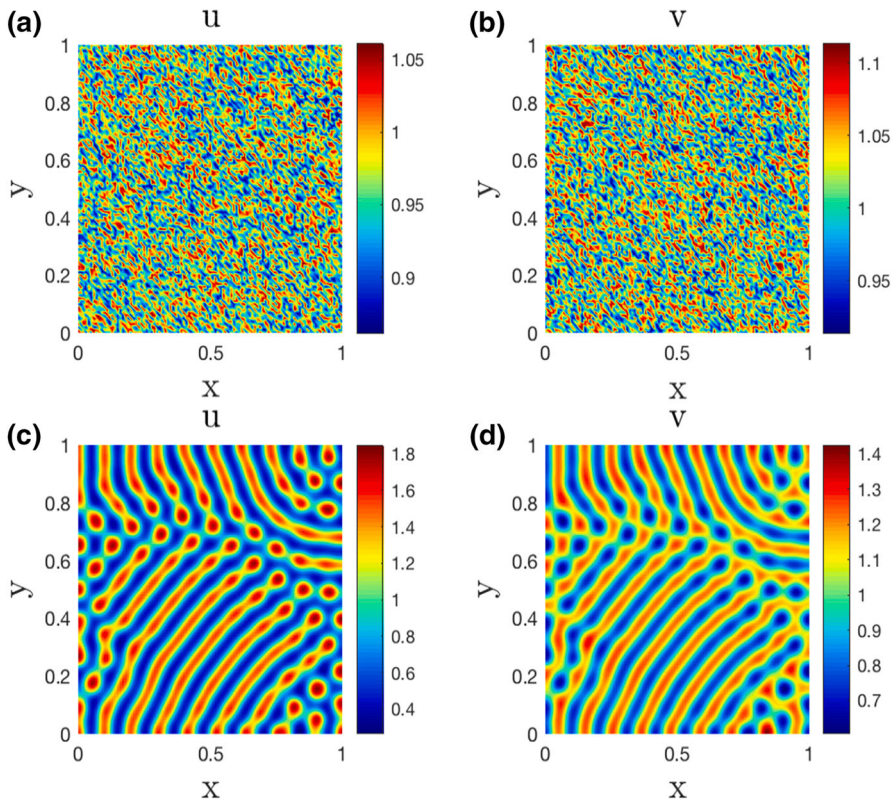
Fig. 4 Spots formation. Turing's instability in u and v for $a = 0.1$, $b = 0.85$, $d = 8$ and $D_u = 0.0025$. **a, b** at $t = 0$ for $\epsilon = 0.01$. **c, d** at $t = 1000$

the spots in the form of this stripe pattern formation accordingly to the full numerical solution of Eqs. (8)–(9) for these model parameters.

For the sake of completeness, we are now developing the standard linear stability analysis of the full PDE system (8)–(9) around the equilibrium solution (u^*, v^*). Our aim is to complement our analysis of the loss of stability of the equilibrium solution that permits the emergence of Turing patterns. To this end, we take the transformations $u(x, y, t) = u^* + e^{\lambda t}\phi(x, y)$ and $v(x, y, t) = v^* + e^{\lambda t}\psi(x, y)$ for sufficiently small functions ϕ and ψ. Thus, Taylor expansions yield the following eigensystem:

$$\lambda \begin{bmatrix} \phi \\ \psi \end{bmatrix} = \underbrace{\begin{bmatrix} D_u \nabla^2 + f_u(u^*, v^*) & f_v(u^*, v^*) \\ g_u(u^*, v^*) & D_v \nabla^2 + g_v(u^*, v^*) \end{bmatrix}}_{\tilde{M}} \begin{bmatrix} \phi \\ \psi \end{bmatrix}, \quad (17)$$

where the eigenfunctions ϕ and ψ satisfy no flux conditions at the boundaries $\phi_x(0, y) = \psi_x(0, y) = 0$, $\phi_x(1, y) = \psi_x(1, y) = 0$ and $\phi_y(x, 0) = \psi_y(x, 0) = 0$, $\phi_y(x, 1) = \psi_y(x, 1) = 0$. The eigenvalue problem stated in Eq. (17) is numerically

Fig. 5 Stripes formation. Turing's instability in u and v for $a = 0.025$, $b = 0.961$, $d = 8$, $D_u = 0.0001$. **a**, **b** at $t = 0$ for $\epsilon = 0.01$. **c**, **d** at $t = 1000$

solved using a second-order central finite difference scheme in the Laplacian operator and in the boundary conditions.

We show in Fig. 6 an example of the linear stability analysis of the equilibrium point located in the Turing's region for $d = 8$. We use the same parameter values as in Fig. 4 where the spots were exhibited. As expected, the equilibrium point has lost stability due to the diffusive interactions. It is also shown the leading unstable eigenvalue $\lambda = 0.011$ and its corresponding eigenfunctions ϕ and ψ which show smooth bumps sufficiently spaced that permit the emergence of spots of activity, as it is shown in Fig. 6.

We now analyze the stability of the equilibrium solution in Turing's region for the parameters used in Fig. 5. In this case, the spectrum contains several unstable eigenvalues, as Fig. 7c, d indicate, while the eigenfunctions ϕ and ψ corresponding to the largest eigenvalue $\lambda = 0.1198$ display sharp peaks positioned close to each other, see Fig. 7a, b. These close packed arrangements give place to the instability that allows the emergence of the stripes. In the next section, we use the Hopf bifurcation property to develop spiral waves which will complement the Turing patterns found in this section.
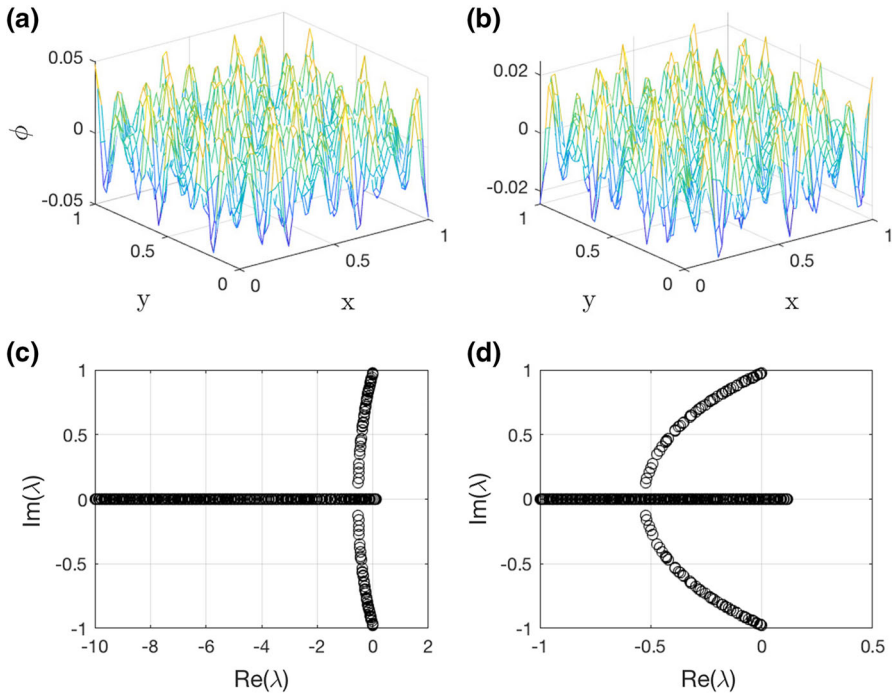
(a)

(b)

(c)

(d)
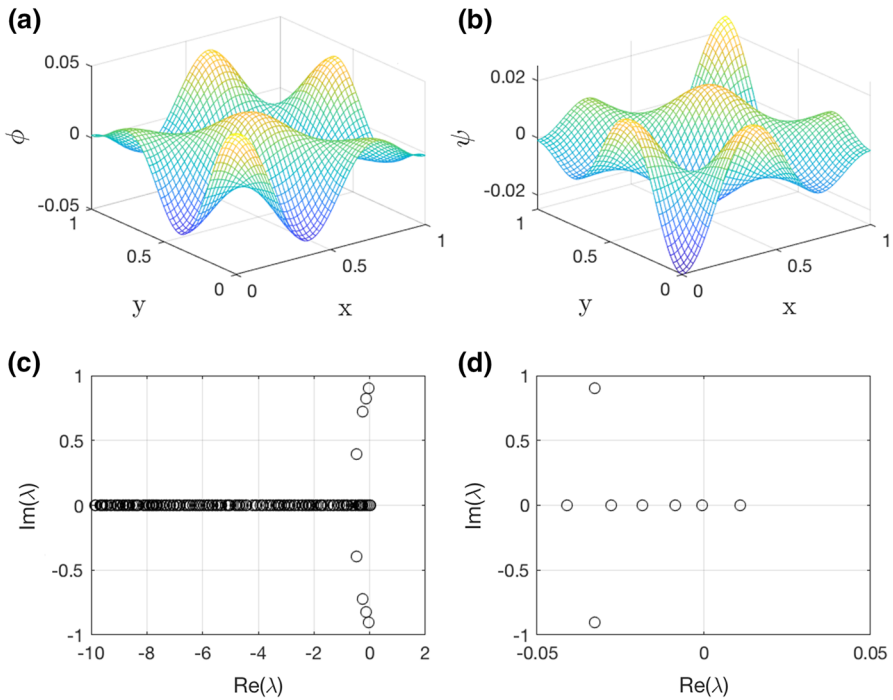
Fig. 6 Linear instability of the equilibrium point for $a = 0.1$, $b = 0.85$, $d = 8$, $D_u = 0.0025$. **a** and **b** Eigenfunctions corresponding to the largest eigenvalue $\lambda = 0.011$. **c** Spectrum. **d** Close up of the spectrum to detect the largest positive eigenvalue

4 Glycolytic Spiral Waves

It is expected that any diffusion-less system exhibiting a Hopf bifurcation experiences, under diffusive interactions, rotating spiral wave solutions (Hagan 1982). Spiral wave solutions in reaction–diffusion systems have been previously investigated in Hagan (1982), Cohen et al. (1978) and Kopell and Howard (1981), among others. Particularly, rotating spiral waves have been numerically observed for glycolytic activity under Goldbeter's approach (Straube et al. 2010). In this section, we focus on numerically establishing a region for the existence of glycolytic spiral solutions to complement the description of pattern formation in the glycolysis process for the two-variable Sel'kov model (8)–(9). To establish such solutions, we first perform a change of variables to Eqs. (8)–(9) to set the equilibrium point (u^*, v^*) at the origin. Spiral wave solutions can be defined by stationary solutions in the rotating polar coordinate frame (r, ϕ), where $\phi = \theta - \omega t$. That is, spiral solutions satisfy the following steady state system in the rotating frame:

$$D_u \nabla_{r,\phi}^2 U^* - \left(U^* + u^*\right) + \left(V^* + v^*\right)\left(a + \left(U^* + u^*\right)^2\right) + \omega \frac{\partial U^*}{\partial \phi} = 0, \quad (18)$$

$$D_v \nabla_{r,\phi}^2 V^* + b - \left(V^* + v^*\right)\left(a + \left(U^* + u^*\right)^2\right) + \omega \frac{\partial V^*}{\partial \phi} = 0, \quad (19)$$

Fig. 7 Linear instability of the equilibrium solution for $a = 0.025$, $b = 0.961$, $d = 8$, $D_u = 0.0001$. **a** and **b** Eigenfunctions corresponding to the largest eigenvalue $\lambda = 0.1198$. **c** and **d**) Spectrum

where $\nabla^2_{r,\phi}$ is the Laplacian operator in polar coordinates and ω is the appropriate rotation frequency of the spiral wave. Since the frequency ω generates, in a general setting, an infinite set of solutions established by all possible spiral rotations, it is necessary to consider an extra pinning condition. This can be done by complementing the system of Eqs. (18)–(19) with the extra conditions $\frac{\partial U^*}{\partial \phi}\mid_{r=R_{\text{fixed}},\phi=\phi_{\text{fixed}}} = 0$, and $\frac{\partial V^*}{\partial \phi}\mid_{r=R_{\text{fixed}},\phi=\phi_{\text{fixed}}} = 0$. The aim of the previous conditions is to analyze a spiral solution by pinning the rotation at a fixed radius and angle, R_{fixed} and ϕ_{fixed}, respectively. Additionally, we consider a bounded domain determined by a circle of sufficiently large radius R, and complement the system with the Neumann boundary conditions $\frac{\partial U^*}{\partial r}\mid_R = \frac{\partial V^*}{\partial r}\mid_R = 0$.

The existence of spiral wave solutions and their stability has been recently studied in Sandstede and Scheel (2002), and examples of spiral wave solutions in reaction–diffusion systems have been rigorously analyzed in Dodson and Sandstede (2019a). The aforementioned authors have also developed a numerical MATLAB routine to determine spiral wave solutions and their stability in bounded domains. The code is available in Dodson and Sandstede (2019b). In this work, we adapted the preceding routine to numerically study the existence of glycolytic spiral solutions. To do so, we discretized space by considering polar nodes consisting of $N_r = 100$ radial and $N_\theta = 200$ azimuthal grid points. We then look for numerical spiral waves determined by the steady state solutions of Eqs. (18)–(19). For instance, Fig. 8a, b shows an
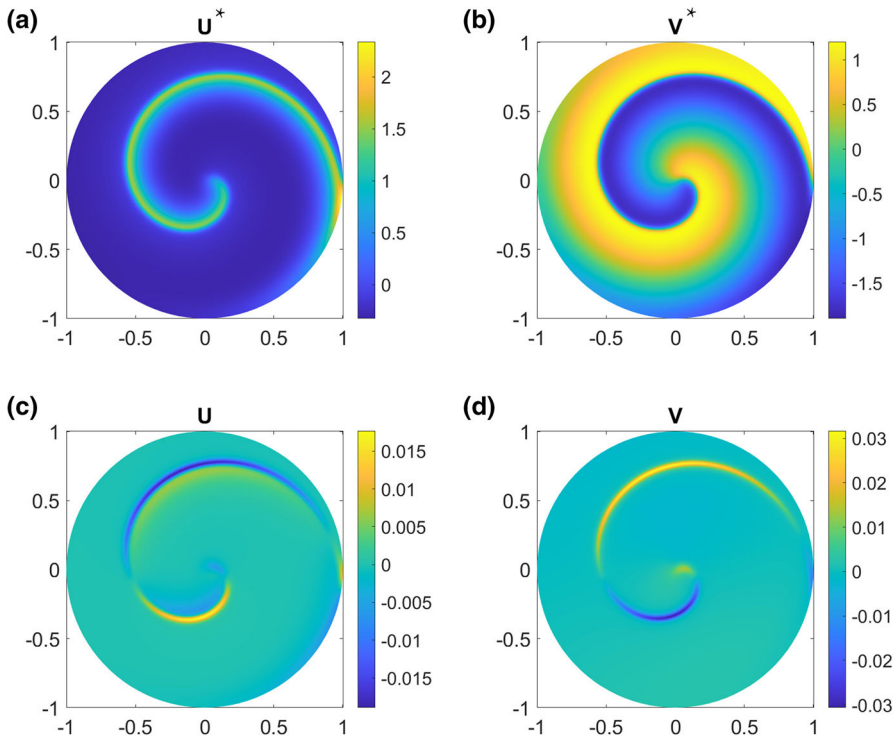
Fig. 8 **a**, **b** Spiral wave U^* and V^* component, respectively, at the steady state. **b**, **c** Linear stability analysis: Real parts of the eigenfunctions associated with translational symmetries $\lambda = 0 + 0.4565i$. Fixed parameters: $a = 0.04$, $b = 0.4$, $D_u = 0.0006$, and $D_v = 0.00001$

example of the substrate and product producing spiral wave solutions according to the model parameters $a = 0.04$, $b = 0.4$, $D_u = 0.0006$ and $D_v = 0.00001$ for the adjusted frequency $\omega = 0.4565$ obtained from the numerical algorithm in the rotating frame. In this case, the spiral solution of the substrate is narrow, whereas the spiral solution of the product is wide.

Once the existence of steady-state solutions in the rotating frame is established, we may study their linear stability by considering whether the dynamics of a perturbation of the steady-state solution remains sufficiently close. To establish the stability problem to be addressed, we let $\mathbf{U}^* = (U^*, V^*)^T$ and $\bar{\mathbf{U}} = (\bar{U}(r, \phi, t), \bar{V}(r, \phi, t))^T$, where $\bar{U}$ and $\bar{V}$ are sufficiently small. We then write the dynamics of the perturbation of the steady state as:

$$\frac{\partial}{\partial t}(\mathbf{U}^* + \bar{\mathbf{U}}) = \omega \frac{\partial}{\partial \phi}(\mathbf{U}^* + \bar{\mathbf{U}}) + \mathbf{D}\nabla_{r,\phi}^2(\mathbf{U}^* + \bar{\mathbf{U}}) + h(U^* + \bar{U}, V^* + \bar{V}), \quad (20)$$

where $h(U, V) = (-(U + u^\star) + (V + v^\star)(a + (U + u^\star)^2), b - (V + v^\star)$ $(a + (U + u^\star)^2))^T$, and $\mathbf{D} = \begin{pmatrix} D_u & 0 \\ 0 & D_v \end{pmatrix}$. By formally linearizing the previous system

around the steady-state solution, and assuming $\bar{U} = e^{\lambda t} U$ and $\bar{V} = e^{\lambda t} V$, we obtain the following eigenvalue problem:

$$\lambda W = \left(\omega \frac{\partial}{\partial \phi} + \mathbf{D} \nabla^2_{r,\phi} + Jh(U^*, V^*) \right) W, \tag{21}$$

where $W = (U, V)^T$ and J denotes the corresponding Jacobian matrix. By differentiating the stationary solution, $\frac{\partial \mathbf{U}^*}{\partial \phi}$, we obtain an eigenfunction of the previous eigenvalue problem with a corresponding zero eigenvalue. This is due to the fact that rotations of the stationary spiral solutions are also spiral solutions. Also, when posed on an infinite domain a pair of complex eigenvalues, $\pm i\omega$, is expected due to translational symmetries of the spiral wave. However, when posed on a finite domain, these eigenvalues are expected to remain numerically close by considering a sufficiently large domain (Barkley 1994). In our work, instabilities due to eigenvalues with positive real part were established for eigenvalues such that $\mathrm{Re}(\lambda) > 10^{-3}$ in correspondence with the order of approximation of the numerical scheme.

The spectrum ensuing from Eq. (21) establishes the linear stability of the spiral wave solution and consists of point eigenvalues and a set determined by the dynamics in the far-field limit. When posed on an unbounded domain, the spectrum is determined by the dynamics of the spiral core and the far-field, whereas when posed on a bounded domain, the boundary effects also determine the spectral properties. The linear and nonlinear stability of spiral wave solutions has been rigorously studied in Sandstede and Scheel (2002) and Dodson and Sandstede (2019a). In particular, in Dodson and Sandstede (2019a), the authors have introduced a methodology to determine the source of instabilities in spiral solutions by analyzing the spectral properties arising from the spiral core, boundary effects, and the far-field limit.

The linear stability of spiral solutions is here addressed only by analyzing the set of leading eigenvalues of the spectra. Following this stability analysis in the examples established in Fig. 8a, b, we find in Fig. 8c, d the real part of the eigenfunctions associated with the pure imaginary eigenvalue $\lambda = 0.4565i$ arising from translation symmetries. Both eigenfunctions resemble the substrate spiral solution. We are thus getting in Fig. 8a, b stable spiral waves of the substrate U and product V. We may actually obtain a stability diagram for fixed diffusivities in the Hopf bifurcation region as it is shown in Fig. 9. To get this picture, we performed a two-parameter numerical continuation based on the stability of steady states of Eqs. (18)–(19) by considering the spiral solutions of Fig. 8a, b as an initial iterate for the fixed diffusivities $D_u = 0.0006$ and $D_v = 0.00001$ and varying the model parameters a and b each time. We note that for such a choice of parameters, there is no coexistence of Turing patterns and spiral solutions since spirals lie inside the Hopf bifurcation region while Turing's condition holds in a small band out of it. As we have mentioned, the existence of spiral waves requires for the diffusivity of the substrate to be faster than the diffusivity of the product in contrast to the Turing pattern conditions previously established.

In Figs. 10 and 11, we provide examples of the loss of stability of the spiral wave solution as point eigenvalues cross the imaginary axis. In Fig. 10, we depict the loss of stability of a spiral solution when the kinetic parameter a is sufficiently low and the source rate is decreased. In this case, as the parameters b decreases, we observe

Fig. 9 Existence region of spiral wave solutions for $R = 1$. The filled and empty points denote linearly stable and linearly unstable spiral solutions, respectively. Fixed parameters: $D_u = 0.0006$ and $D_v = 0.00001$
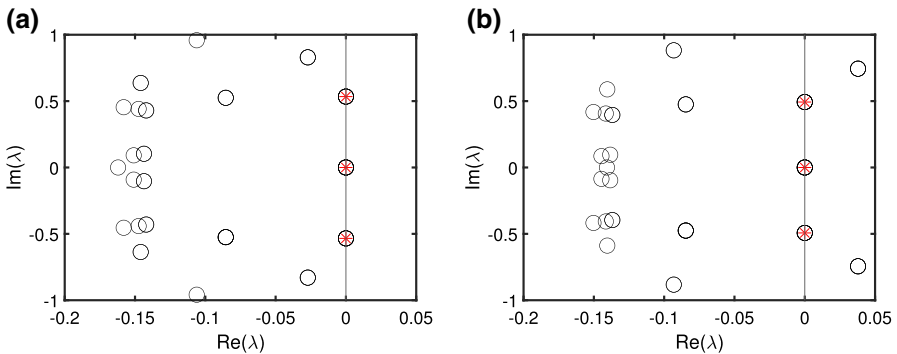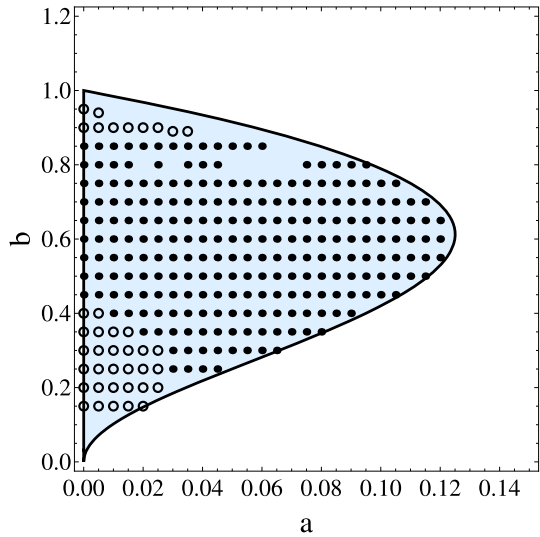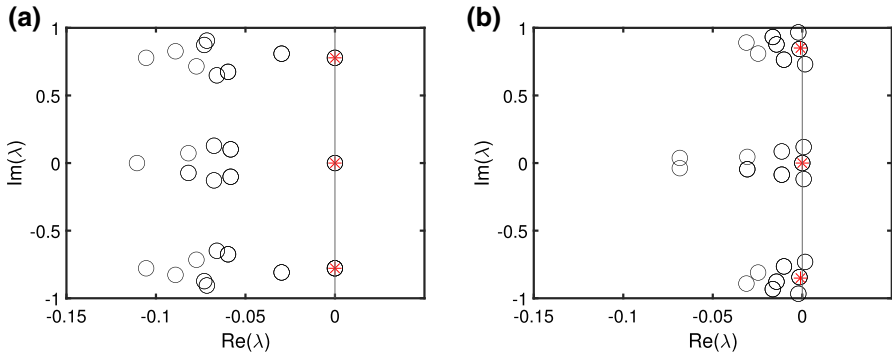

Fig. 10 Spiral wave solution loses stability through a Hopf bifurcation. The black circles denote point eigenvalues of the spiral solution and the red marks denote the eigenvalues associated with the translational and rotational invariance of the spiral solution. The black line determines $\text{Re}(\lambda) = 0$. As the parameter b decreases, the spiral solution loses stability. **a** $a = 0$ and $b = 0.45$. **b** $a = 0$ and $b = 0.4$. Fixed parameters: $D_u = 0.0006$ and $D_v = 0.00001$

an isolated conjugate pair of eigenvalues crossing the imaginary axis and producing a Hopf bifurcation. On the other hand, we observe in Fig. 11 the loss of stability of the spiral solution when the kinetic parameter a is sufficiently low, and the source rate is increased. In this case, there is an accumulation of eigenvalues on the imaginary axis near the eigenvalues corresponding to the translational and rotational properties of the wave solution. Eventually, the accumulated eigenvalues start to cross the imaginary axis and the spiral solution becomes linearly unstable.

Finally, we aim to numerically validate the existence region for the spiral solutions established in Fig. 9. Our purpose is to recover the spiral dynamics and some of their features in the full reaction–diffusion system. To do so, we numerically solve the complete glycolytic model determined in Eqs. (8)–(9) by considering the model

Fig. 11 Spiral wave solution loses stability. The black circles denote point eigenvalues of the spiral solution and the red marks denote the eigenvalues associated with the translational and rotational invariance of the spiral solution. The black line determines $\text{Re}(\lambda) = 0$. As the parameter b increases, the spiral solution loses stability. **a** $a = 0$ and $b = 0.85$. **b** $a = 0$ and $b = 0.9$. Fixed parameters: $D_u = 0.0006$ and $D_v = 0.00001$
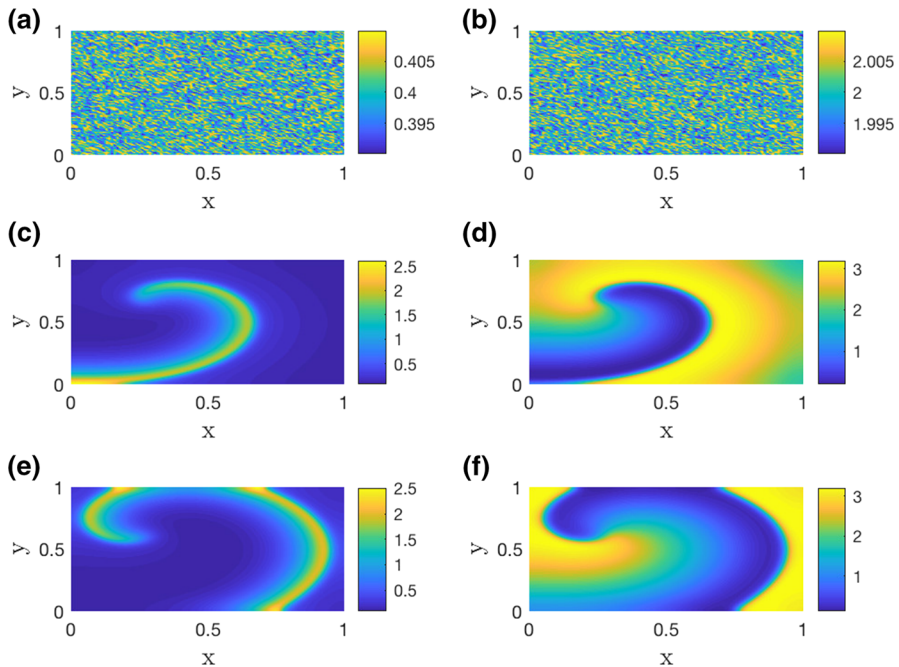
Fig. 12 Spiral wave solutions obtained from the full numerical solution of Eqs. (8)–(9) for the model parameters $a = 0.04$, $b = 0.4$, $D_u = 0.0006$, $D_v = 0.00001$, $\delta t = 0.001$ and $\delta x = \delta y = 0.01$. Evolution of u at **a** $t = 0$ for $\epsilon = 0.01$, **c** $t = 800$ and **e** $t = 1300$. Evolution of v at **b** $t = 0$ for $\epsilon = 0.01$, **d** $t = 800$ and **f** $t = 1300$

parameters that were used to produce the stable spirals of Fig. 8a, b, that is, $a = 0.04$, $b = 0.4$, $D_u = 0.0006$ and $D_v = 0.00001$. In Fig. 12, we successfully recover spiral solutions for the full system of equations. In this figure, we see how an equilibrium solution randomly perturbed at $t = 0$ evolves to a single armed solution for both the substrate, Fig. 12c, e, and the product, Fig. 12d, f.

(a)

(b)

(c)
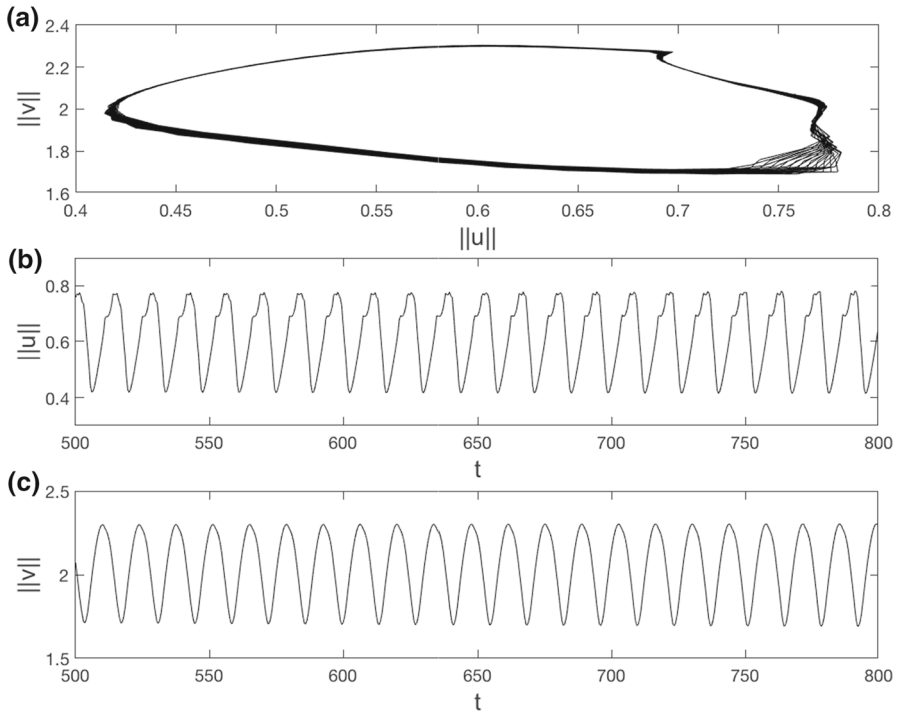
Fig. 13 **a** Phase diagram of the spiral wave rotation determining a closed loop in the $||u||$vs$||v||$ plot that suggest periodicity of the solution. **b**, **c** $||u||$ and $||v||$, respectively. The motion of **b** and **c** suggest that the solutions display periodic oscillations. The estimated dominant frequency of oscillations is $\omega = 0.46$. Fixed parameters: $a = 0.04$, $b = 0.4$, $D_u = 0.0006$ and $D_v = 0.00001$

In order to get more insight about the dynamics of these solutions, we follow the idea developed in Amdjadi (2010) by computing the time-dependent Euclidean norms determined by $||u|| = \left(\int_0^1 \int_0^1 | u(x, y, t) |^2 \, dx dy \right)^{\frac{1}{2}}$ and $||v|| = \left(\int_0^1 \int_0^1 | v(x, y, t) |^2 \, dx dy \right)^{\frac{1}{2}}$ for convenient discretizations of the numerical solutions u and v. Our aim is to extract feature dynamics of the solutions by analyzing their corresponding norms in the whole spatial domain looking for a global behavior of the rotating waves. We point out that a local analysis of the solutions can be made by numerically following the spiral tips; however, this idea is more difficult to implement. In Fig. 13a, we depict the phase diagram of the spiral rotation waves obtained in Fig. 12, and we recover a closed loop in the $||u||$vs$||v||$ diagram. This result suggests that the rotating spiral waves u and v, displayed in Fig. 12, are periodic. Also, in Fig. 13b, c, we show the evolution of the norms $||u||$ and $||v||$, respectively, between the times $t = 500$ and $t = 800$ where the dynamics of the spiral solutions are well-defined. From these two figures, it is clear the periodicity of the oscillations which agrees with the expected features of the spiral rotations. Furthermore, by performing a Fourier analysis of these periodic norms, we recover a dominant frequency of $\omega = 0.46$ which is in concordance with the frequency previously obtained for these

spiral solutions in Fig. 8. In this way, we are able to relate feature dynamics of periodicity and frequency from the spiral waves described as steady state solutions of Eqs. (18)–(19) to the numerical solutions of the full reaction diffusion system (8)–(9), thus validating our previous findings.

5 Discussion and Concluding Remarks

Reaction–diffusion systems are commonly used to exhibit the existence, or to describe the conditions for the appearance of spatiotemporal activity patterns. In his fundamental work, Turing (1952), Alan Turing established that under specific conditions and convenient difference of diffusion rates of the underlying chemicals, stable activity patterns can arise. Different works have generalized the efforts developed by Turing, and have established some conditions for pattern formation, specifically in glycolytic processes. For example, in Strier and Dawson (2007), the authors established the existence of cell-sized Turing spots in the five-variable Sel'kov model by using parameter values in agreement with experimental observations. In their work, they used the same diffusion coefficient for both ATP and ADP. Under this scenario they proposed that Turing patterns are mainly regulated by the enzyme concentration and the intrinsic glycolytic flux. They suggested that Turing patterns could play a part during the cell division process in eukaryotic cells. Moreover, they proposed that the pattern size (and as a consequence the number of spots) could be determined by the glycolytic flux. In this way, their work established possible connections between oscillations, pattern formation and key features in the glycolytic pathway. In comparison, in our work, we have established parameter ranges for Turing pattern formation that are directly determined by the diffusion rates. In our simplified modeling scenario, it is imperative to have unequal diffusion rates to obtain Turing pattern formation. This discrepancy with the aforementioned model could be due to the change of order of magnitude of the diffusion and reaction terms in the reduction in the enzyme variables (fast variables) from the $five$-variable Sel'kov model to the two-variable Sel'kov model (Strier and Dawson 2004). Nevertheless, our work generalizes the existence of not a single set of parameters, but rather a range of parameters that support pattern formation and, that are connected to the emergence of glycolytic oscillations. That is, under convenient diffusion the parameter ranges for glycolytic oscillations (Hopf bifurcation region in Fig. 1), provides a lower bound for Turing pattern regions (blue region in Fig. 3). As suggested by numerical evidence from Strier and Dawson (2007), our work determines that both the glycolytic flux (model input flux and rate constants) and the ATP and ADP established an estimate of the number of spots present. In particular, our results strengthens the hypothesis that the glycolytic pathway can play a role in the processing of biological information. Therefore, we established the theoretical setting that estimates the number of spots that can plausibly fit a cell during the division process. This is also in concordance with experimental evidence that shows the influence of glycolytic flux on the organogenesis stage in mouse embryos (Bulusu et al. 2017). Additionally, different works in the literature have also studied the conditions for pattern formation in glycolytic models. In Prigogine et al. (1969), the authors established that the emergence of Turing patterns was restricted to the case where the substrate

ATP and the product ADP diffused at adequately different rates. This result is in agreement with our observations. Also, in Hasslacher et al. (1993), Turing patterns in a glycolytic model were presented in the case where the substrate was diffusing 25 times faster than the product. The previous assumption was intuitively problematic, due to the expected similar dynamics of both the substrate and the product during the enzymatic reaction. In comparison to the previously mentioned research, our work provides a complete description on the conditions of the diffusivity rates that allow for the emergence of Turing patterns. In particular, we have established a region for Turing instabilities depending on the choice of the diffusion coefficients. Numerical analysis of our conditions established that in order for Turing patterns to emerge the diffusivity of the product needs to be at least 6.2 times faster than the diffusivity of the substrate. Also, the source rate b needs to be sufficiently large and the kinetic parameter a needs to be sufficiently low. The difussivity rates that we found are in agreement with the observations established in Strier and Dawson (2007) and Prigogine et al. (1969). More recently, in Basu and Bhattacharjee (2020), the authors established a rigorous mathematical analysis of a glycolytic model that determines that a uniform oscillatory state, or a periodic pattern, could emerge according to the choice of initial conditions and the diffusivities of the substrate and the product. In comparison with the aforementioned works, we have provided explicit parameter relations that connect the emergence of glycolytic oscillations and pattern formation.

As it has been previously mentioned, there is evidence of the existence of in vitro spiral NADH waves during glycolytic experiments in yeast extracts (Vermeer 2008; Mair and Müller 1996; Mair et al. 2001). However, as far as the authors are aware, the mathematical modeling of such glycolytic patterns and their linear stability has not been formerly addressed. In our work, we have been able to establish the existence of spiral wave solutions in a spatially extended glycolytic model. Also, we have analyzed the effect of the model parameters on the stability of the spiral solutions. Our results showed that in general, as we tend toward a diminished rate constant of the low activity enzyme state in a cell ($a \to 0$), and the source rate b is varied, the spiral wave solution loses stability by means of a Hopf bifurcation regarding the full PDE. Our results on the existence of spiral solutions established that it might be necessary a 60 times faster diffusivity of the substrate in comparison with the diffusivity of the product to allow for the emergence of glycolytic spirals. This also suggests that the conditions for Turing patterns and spiral waves are exclusive among them. This is consistent with experimental evidence realized in open spatial reactors established in Vermeer (2008). Here, it is described a transition from propagating waves to complex patterns; among them, stationary Turing-like patterns such as dot waves; to spiral waves. In Vermeer (2008) and Müller et al. (1985, 1987), the experimental conditions for Turing-like patterns were determined by a change in the protein content. However, there is also experimental evidence of a connection between protein content and glycolytic flux (Yagi et al. 2021). Thus, our results support that indeed, the glycolytic flux determines the spatial patterns obtained under experimental conditions by a difference in protein content.

In summary, this work provides a novel description of parameter conditions necessary for the emergence of patterns in a simplified two-variable glycolytic model. However, the problem of establishing parameter conditions for the emergence of such

patterns in more realistic glycolytic models containing more accurate biochemical descriptions, including the five-variables Sel'kov's model, still remains open. Due to the believed role of pattern formation on biological information processing, it is of key importance to determine the exact conditions that allow the emergence of different patterns during the glycolytic pathway. Although our work cannot provide parameter ranges that quantitatively describe observable patterns in glycolytic experimental settings, it does provide a qualitative description of the relation between the model parameters that allow for the emergence of distinct patterns. Additionally, our parameter ranges might determine qualitative glycolytic dynamics necessary for the propagation direction of activated neutrophil cells as suggested in Petty et al. (2000). As a consequence of our analysis, the question can be posed of whether activated neutrophil cells can have propagation directions in the form of spiral rotating waves, as it is observed in this glycolytic model. Future research directions can be directed to establishing the conditions for the propagation of traveling waves, and their stability, of glycolytic activity. Therefore, there is still ample dynamics that needs to be investigated to establish a complete description of the mathematical models that are used to describe glycolytic dynamics.

References

Amdjadi F (2010) A numerical method for the dynamics and stability of spiral waves. Appl Math Comput 217:3385

Ashkenazi M, Othmer HG (1978) Spatial patterns in coupled biochemical oscillators. J Math Biol 5:305

Barkley D (1994) Euclidean symmetry and the dynamics of rotating spiral waves. Phys Rev Lett 72:164

Basu A, Bhattacharjee JK (2020) When Hopf meets saddle: bifurcations in the diffusive Selkov model for glycolysis. arXiv:2004.10687

Bier M, Bakker BM, Westerhoff HV (2000) How yeast cells synchronize their glycolytic oscillations: a perturbation analytic treatment. Biophys J 78:3

Bulusu V, Prior N, Snaebjornsson MT, Kuehne A, Sonnen KF, Kress J, Stein F, Schultz C, Sauer U, Aulehla1 A (2017) Dev Cell. **40**(4):331–341

Casem ML (2016) Case studies in cell biology. Academic Press, New York

Chow SN, Mallet-Paret J (1977) Integral averaging and bifurcation. J Differ Equ 26:112

Cohen DS, Neu JC, Rosales RR (1978) Rotating spiral wave solutions of reaction–diffusion equations. SIAM J Appl Math 35:3

Corkey BE, Tornheim K, Deeney JT, Glennon MC, Parker JC, Matschinsky FM, Ruderman NB, Prentki M (1988) Linked oscillations of free Ca^{2+} and the ATP/ADP ratio in permeabilized $RINm5F$ insulinoma cells supplemented with a glycolyzing cell-free muscle extract. J Biol Chem 263(9):4254–8

Dodson S, Sandstede B (2019a) Determining the source of period-doubling instabilities in spiral waves. SIAM J Appl Dyn Syst 18:2202

Dodson S, Sandstede B (2019b) GitHub repository: spiral waves, boundary sinks, and spectra. https://github.com/sandstede-lab/Spiral-Waves-Boundary-Sinks-and-Spectra,

Goldbeter A (1996) Biochemical oscillations and cellular rhythms: the molecular bases of periodic and chaotic behaviour. Cambridge University Press, Cambridge

Goldbeter A, Lefever R (1972) Dissipative structures for an allosteric model. Application to glycolytic oscillations. Biophys J 12:1302

Gray P, Scott SK (1990) Chemical oscillations and Instabilities. Clarendon Press, Oxford

Hagan PS (1982) Spiral waves in reaction–diffusion equations. SIAM J Appl Math 42:762

Hasslacher B, Kapral R, Lawniczak A (1993) Molecular Turing structures in the biochemistry of the cell. Chaos 3:7

Hess B, Boiteux A (1971) Oscillatory phenomena in biochemistry. Annu Rev Biochem 40:237

Higgins J (1964) A chemical mechanism for oscillation of glycolytic intermediates in yeast cells. Proc Natl Acad Sci US 51:989

Higgins J (1965) In control of energy metabolism (edited by B. Chance et al). Academic Press, New York and London

Kopell N, Howard LN (1981) Target pattern and spiral solutions to reaction–diffusion equations with more than one space dimension. Adv Appl Math 2:417

Mair T, Müller SC (1996) Traveling NADH and proton waves during oscillatory glycolysis in vitro. J Biol Chem 271:2

Maini PK, Painter KJ, Chau HNP (1997) Spatial pattern formation in chemical and biological systems. J Chem Soc Faraday Trans 93:3601

Mair T, Warnke C, Müller SC (2001) Spatio-temporal dynamics in glycolysis. Faraday Discuss 120:249–259

Müller SC, Plesser T, Hess B (1985) Surface tension driven convection in chemical and biochemical solution layers. Ber Bunsen-Ges Phys Chem 89:654–658

Müller SC, Plesser T, Hess B (1987) Three-dimensional representation of chemical gradients. Biophys Chem 26:357–365

Murray DB, Beckmann M, Kitano H (2007) Regulation of yeast oscillatory dynamics. PNAS 104:7

Nicolis G, Prigogine I (1977) Self-organization in nonequilibrium systems. Wiley, New York

Olsen LF, Degn H (1978) Oscillatory kinetics of the peroxidase-oxidase reaction in an open system. Experimental and theoretical studies. Biochim Biophys Acta 523:321

Petty HR, Worth RG, Kindzelskii AL (2000) Imaging sustained dissipative patterns in the metabolism of individual living cells. Phys Rev Lett 84(12):2754–7

Prigogine I, Lefever R, Goldbeter A, Herschkowitz-Kaufman M (1969) Symmetry breaking instabilities in biological systems. Nature 223:913

Sanders JA, Verhulst F (1985) Averaging methods in nonlinear dynamical systems. Springer, Berlin

Sandstede B, Scheel A. Spiral waves: linear and nonlinear theory. arXiv:2002.10352 (2002)

Sel'kov EE (1968) Self-oscillations in glycolysis. Eur J Biochem 4:79

Straube R, Vermeer S, Nicola EM, Mair T (2010) Inward rotating spiral waves in glycolysis. Biophys J 99:L04

Strier DE, Dawson SP (2004) Role of complexing agents in the appearance of Turing patterns. Phys Rev E Stat Nonlin Soft Matter Phys 69(6 Pt 2):066207

Strier DE, Dawson SP (2007) Turing patterns inside cells. PLoS ONE 2(10):e1053

Strikwerda John C. (2012) Finite difference schemes and partial differential equations, 2nd edn. Society for Industrial and Applied Mathematics, New York. https://doi.org/10.1137/1.9780898717938

Strogatz SH (1994) Nonlinear dynamics and chaos: with applications to physics. Chemistry, and engineering. Perseus Books Biology, New York

Turing AM (1952) The chemical basis of morphogenesis. Philos Trans R Soc Lond Ser B 237:37

Vermeer S (2008) Spatio-temporal dynamics of glycolysis in an open spatial reactor. Ph.D. thesis, Magdeburg Univ

Voet D, Voet JG, Pratt CW (2006) Fundamentals of biochemistry, 2nd edn. Wiley, New York

Weber A, Zuschratter W, Hauser MJB (2020) Partial synchronisation of glycolytic oscillations in yeast cell populations. Sci Rep 10:19714

Yagi H, Kasai T, Rioual E, Ikeya T, Kigawa T (2021) Molecular mechanism of glycolytic flux control intrinsic to human phosphoglycerate kinase. PNAS 118(50):e2112986118

Zaikin AN, Zhabotinsky AM (1970) Concentration wave propagation in two-dimensional liquid-phase self-oscillating system. Nature 225:535–537